Dynamic Modeling and Control of the Magplane Vehicle

(*) Jiarong Fang, (*) Alexey Radovinsky, (**) D. Bruce Montgomery
(*) MIT Plasma Science and Fusion Center, 185 Albany Street, Cambridge, MA 02139, USA
617-253-3731, fang@psfc.mit.edu, 617-253-8152, radovinsky@psfc.mit.edu
(**) Magplane Technology, Inc. 380 Hanscom Drive, Bedford, MA 01730, USA
617-253-5552, montgomery@magplane.com

Keywords

Maglev, EDS, Vehicle Dynamic Modeling, Simulation

Abstract

This paper describes a 3D dynamic simulation model that was developed to simulate and control the dynamic response of the magnetically levitated Magplane vehicle subject to periodic guideway disturbances, vertical and lateral accelerations in curves, and strong side wind forces. In the 3D simulation model, because both pitch angle and yaw angle of the vehicle are very small, a distributed control system was used to independently control the front and rear of the vehicle. By applying active control strategies in the secondary suspension system which supports lift pads, the ride quality was significantly improved.

1 Introduction

The ride quality of vehicle dynamics has been recognized as crucial to the commercial success of passenger-carrying transportation systems [1]. The Magplane is an inherently stable electrodynamic suspension (EDS) system with many updated characteristics from the 1992 System Concept Definition for the US National Maglev Initiative [2-6], such as a Linear Synchronous Motor (LSM) with Halbach-array propulsion permanent magnets, the arc-shape guideway, electromagentic switches and control systems, and Halbach-array lift pad permanent magnets and 2 cm aluminum sheet. However, in view of the well-known under-damped nature of EDS-type maglev systems [7-9], an active electromagnetic actuator parallel with passive spring and damper is employed between lift pads and vehicle body in order to isolate the vehicle from the guideway periodic disturbance and vehicle body displacements when traversing the curves and encountering strong side winds.

2 Vehicle Configuration

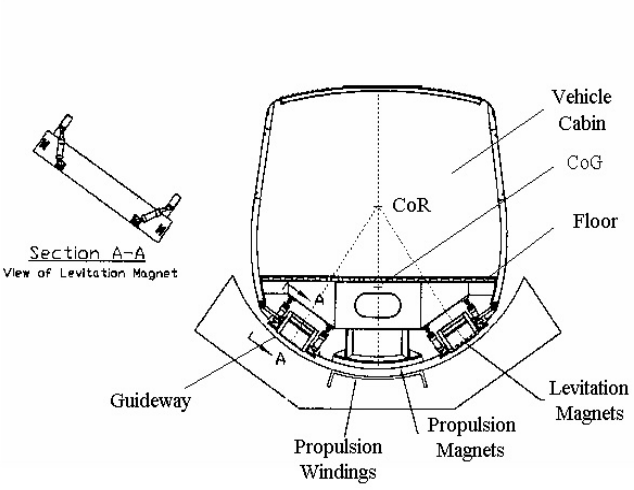

Fig. 1 Front View of Vehicle and Guideway

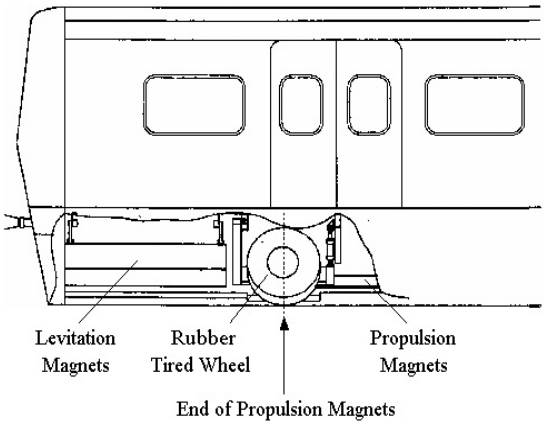

Fig. 2 Side View of Vehicle

Figure 1 and 2 show the front and side views of the Magplane vehicle. The vehicle is a symmetric model which consists of a 10 wavelength propulsion array located at the center of the vehicle bottom, and four identical 2 wavelength lift pads symmetrically located at four corners of the vehicle with the same tilted 37 degree angle against the vertical plane due to the arc-shaped guideway. The propulsion and lift pad arrays are composed of Halbach-array permanent magnets with consecutively clockwise rotated 45 degree of magnetization directions in the plane of the vehicle motion and vertical direction. The detailed vehicle specifications are listed in Table 1. The vehicle body is about 16.4m long, 3.3m wide and 3.6m high. The vehicle floor is about 1.1m above the propulsion magnet array and the center of the each tilted lift pad is about 0.8m below the vehicle floor.

Table 1. Vehicle specifications

Parameter	**Nomenclature**	**Value**
Vehicle dimension		
Length	L_V	16.4 m
Width	W_V	3.3 m
Height	H_V	3.6 m
Vehicle weight		
Empty weight	M_o	$23*10^3$ kg
Normal passenger-loaded weight	M_n	$31.2*10^3$ kg
Crush passenger-loaded weight	M_c	$36*10^3$ kg
Each lift pad assembly (4 sets)	m_l	$1.6*10^3$ kg
Propulsion magnet assembly	m_p	$6.0*10^3$ kg
Center of Rotation (CoR)	CoR	+2.0 m relative to vehicle bottom surface
Nominal operating gap	G	0.1 m
Center of Gravity (CoG)	CoG	
Empty	CoG_o	-1.4 m relative to CoR
With normal passengers	CoG_n	-1.0 m relative to CoR
With crush passengers	CoG_c	-0.8 m relative to CoR

3 Vehicle Dynamic Modeling

3.1 Vehicle Dynamic model

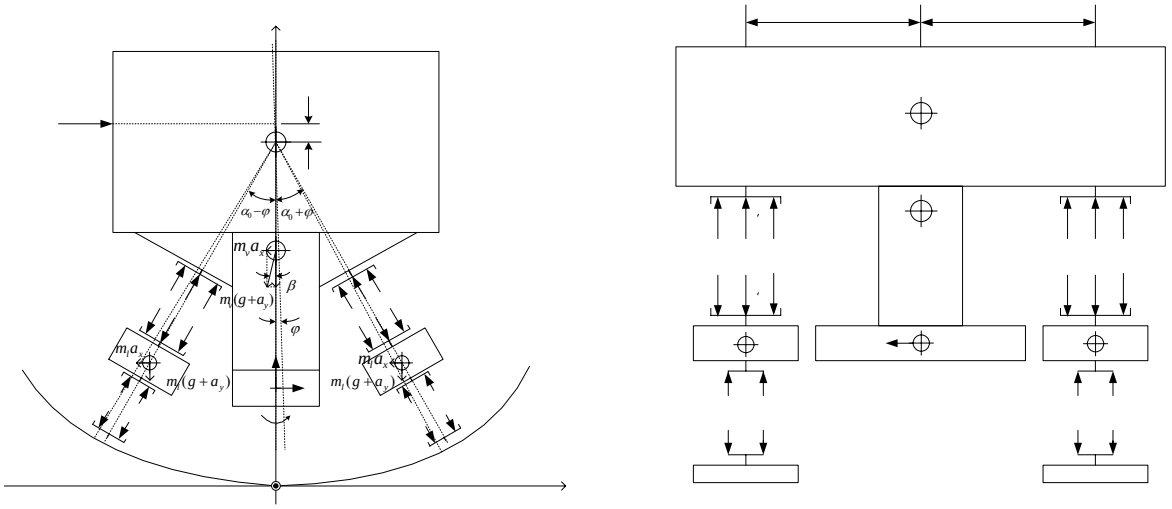

The front and side view of vehicle force model are shown in Figure 3 and 4, respectively. The 37 degree orientation of the lift pad magnets produce both lift and lateral guidance. Suppose the vehicle is subject to the periodic guideway disturbance force *Fd*, both vertical and lateral accelerations a_x, and a_y in curving performance, and the strong side wind force *Fw*. There is an active actuator plus passive secondary suspension system between the vehicle cabin and the lift pad, and here the force F_A is used to represent the force of this actuator. For force subscriptions, A means actuator force, K denotes spring, D damping, d guideway disturbance, w wind disturbance, k keel effect from propulsion magnets, and p propulsion force. For different suspensions, P signifies primary suspension, and S secondary suspension. For different locations, f and r mean front and rear sides, and 1 and 2 mean left and right sides.

3.2 Vehicle Control Model

In this 3D simulation model, because pitch angle and yaw angle of the vehicle are very small, we could use the distribution control system to control the front and rear vehicle independently and apply two kinds of active control strategies in the secondary suspension system. One strategy is to use acceleration feedback control to reduce the vertical and lateral accelerations of vehicle body which are dominant in the ride quality [10-11], and the second is to compensate the large displacement of soft springs of the secondary suspension caused by inertial forces associated with performance in the curves and under strong wind forces in order to keep deviation of the rotation center of vehicle at a minimum and make the vehicle stable.

3.2.1 Acceleration feedback control

The acceleration of vehicle can be measured by an accelerometer, backfed through a gain box Ka, and finally implemented by an electromagnetic active component parallel with the passive suspension system to apply the identical active force to both vehicle and lift pad in opposite directions. In this 3D vehicle model, however, the left and right primary magnetically levitated suspensions, front lift pads, and secondary suspension have opposite tilting angle against the horizontal plane due to arc-shaped guideway. As shown in Figure 5, we use the acceleration a_R, and a_L along those tilting angle directions to represent the vertical and horizontal accelerations of vehicle, a_x, and a_y, by using following equations:

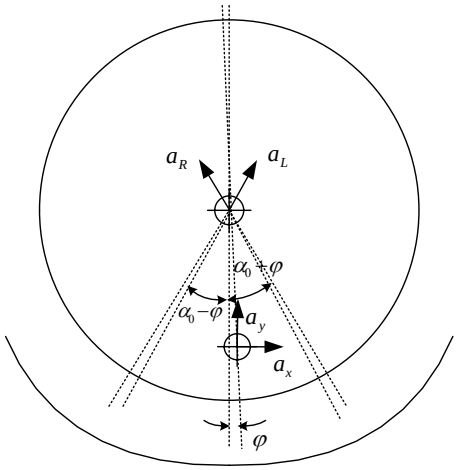

$$\begin{cases} a_L = \left[a_y \sin(\alpha_0+\varphi) + a_x \cos(\alpha_0+\varphi)\right] / \sin(2\alpha_0) \\ a_R = \left[a_y \sin(\alpha_0-\varphi) - a_x \cos(\alpha_0-\varphi)\right] / \sin(2\alpha_0) \end{cases} \quad (1)$$

Then we can improve the ride comfort quality by reducing the acceleration along those tilting angle directions through the acceleration feedback control.

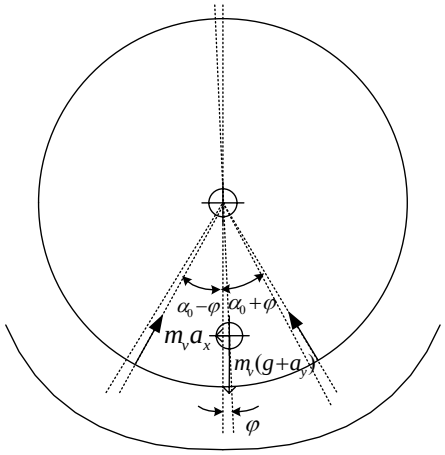

3.2.2 Length Compensation Control

The vehicle will have a large deviation from the center of rotation due mainly to the large displacement of soft springs of the secondary suspension caused by inertial forces associated with curving performance and the strong wind force. The length compensation control is to compensate large displacement of soft springs of the secondary suspension and under whatever influence of the d'Alambert forces its center of the mass is still in the same position as in the stable

condition. As shown in Figure 6, from the equations of equilibrium, $\sum F_x = 0$, $\sum F_y = 0$, the left and right compensation control forces $F_{NL} - F_0$, and $F_{NR} - F_0$ can be represented by following equations:

$$\begin{cases} F_{NL} = [m_v(g + a_y)\sin(\alpha_0 + \varphi) + m_v a_x \cos(\alpha_0 + \varphi)]/\sin(2\alpha_0) \\ F_{NR} = [m_v(g + a_y)\sin(\alpha_0 - \varphi) - m_v a_x \cos(\alpha_0 - \varphi)]/\sin(2\alpha_0) \\ F_0 = m_v g/(2\cos\alpha_0) \end{cases} \tag{2}$$

3.3 Disturbance Model

3.3.1 Guideway Sagging

As shown in Figure 7, the guideway sheet resides on concrete slabs periodically supported in the motion direction with arc sagging distance of 2δ for a typical concrete slab length of L. Assume that this deviation from flatness can be presented as a sine function of the distance, S, in the direction of motion, then the periodic guideway disturbance force can be represented as

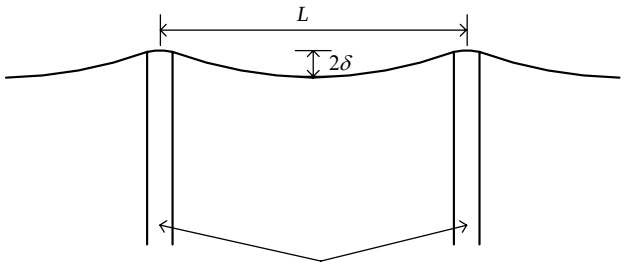

$$F_d = k\delta \sin(2\pi \frac{S}{L}) \tag{3}$$

where k is the magnetic suspension spring constant.

3.3.2 Curving Performance

The lateral acceleration a_x and vertical acceleration a_y can be set as two different sine functions to simulate various sine-curve turns and uphill/downhill by choosing different values of parameters n_x, and n_y in the following formulae

$$a_x = a_{x0} Sin(n_x \pi t / t_{\max}) \ , \ a_y = a_{y0} Sin(n_y \pi t / t_{\max}) \tag{4}$$

where different n_x and n_y represent different situations. Here we choose n_x=5 and n_y=2, which corresponds to predominantly lateral turns.

3.3.3 Wind Force

As shown in Figure 8, two strong gusts of wind with peak speed of 19m/s are applied to the model at a point 0.5m above the center of rotation (CoR). The shape function of the time could be described as

$$F_w = Mg \sum_{n=1}^{2} \frac{fw_n}{r_n} \ Sech[\sigma_n (t - t_n)] \tag{5}$$

where fw_1/r_1=0.0925, fw_2/r_2=-0.0925, $\sigma_1 = \sigma_2 = 1s^{-1}$, t_1=10s, and t_2=40s.

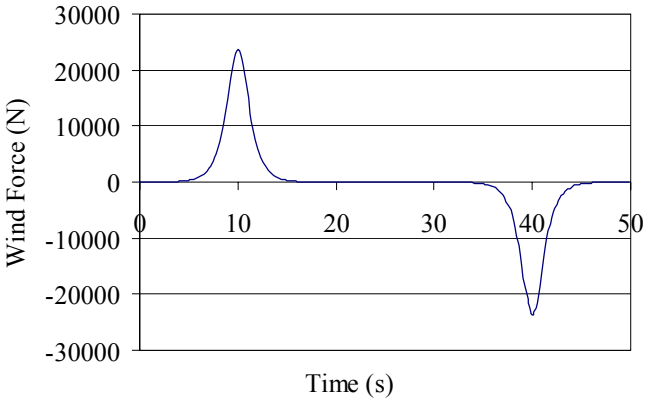

Fig. 8 Strong Wind Forces

4 3D Vehicle Model Simulation

We use MATLAB SimMechanics to build up the 3D vehicle simulation model running up to 50m/s as an intra-city transportation system. Here we assume that the propulsion force Fpz is always kept in the motion direction and does not use the LSM phase control. We suppose that the vehicle is accelerated from the initial zero condition at a constant acceleration, a=0.1g, until it reaches the cruise speed, Vc=50 m/s, at the time point of 50s.

Figure 9 and 10 show lateral and vertical displacements and accelerations of the CoR at both front and rear of the vehicle. Results indicate that the dynamic response of the front CoR is very similar to that of the rear CoR. There are two peak responses in both displacements and accelerations, especially in the lateral displacements, which correspond to the strong side wind gusts with the speed of 19m/s at the time of 10s and 40s. The length compensation control compensates the large displacement of soft springs of the secondary suspension caused by strong wind gusts and vertical and lateral accelerations in the curves. The maximum lateral displacement offset from the nominal vehicle's CoR during the first strong gust of wind is about 0.09m and the vertical displacement is about 0.03m, all of which are less than the lateral and vertical gaps, so the vehicle body will never touch the guideway even during the strong wind gusts. The lateral and vertical accelerations of both front and rear vehicle's CoR also have a peak value around the time point of 15s (at the velocity of 15m/s) which is caused by the secondary suspension resonant frequency of 0.5 Hz. Small constant vibrations in the vertical acceleration are caused by the periodic guideway disturbance and are reduced significantly by the acceleration feedback control. The maximum lateral acceleration of 0.23m/s^2 and the maximum vertical accelerations of 0.33m/s^2 are within the lateral vibration limitation of 0.027g (0.26m/s^2) and vertical vibration limitation of 0.035g (0.34m/s^2) in 1-hour reduced comfort of ISO Standard 2631 [11], so even under the strong wind gusts and resonant frequency, the acceleration feedback control will ensure the vehicle meets good ride comfort.

As shown in Figure 11, the roll angle is closely follows the natural banking angle (beta angle). Even under strong wind gusts, the maximum angle error is about 0.5 degree. The Magplane guideway can always keep the propulsion windings in the center of the guideway bottom without need to tilt the guideway in curves. This reduces the cost of the guideway relative to other maglev systems which require a specific guideway tilting angle design according to the curves and the speed profile.

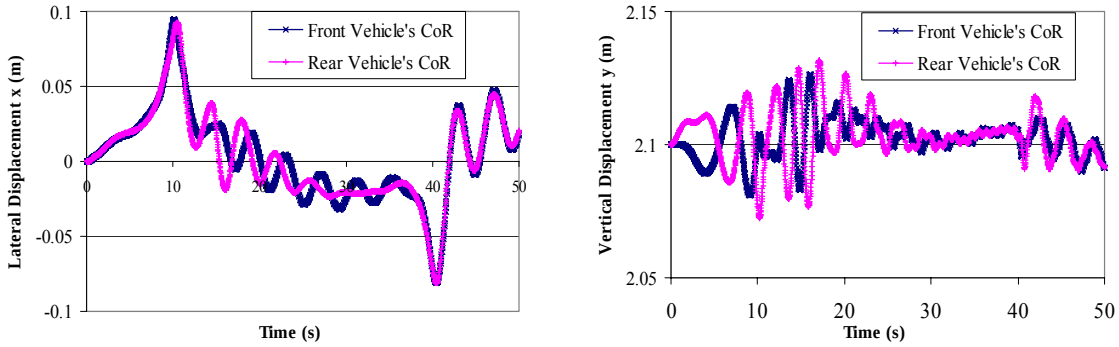

Fig. 9 Lateral and Vertical Displacements of Front and Rear Vehicle's CoR

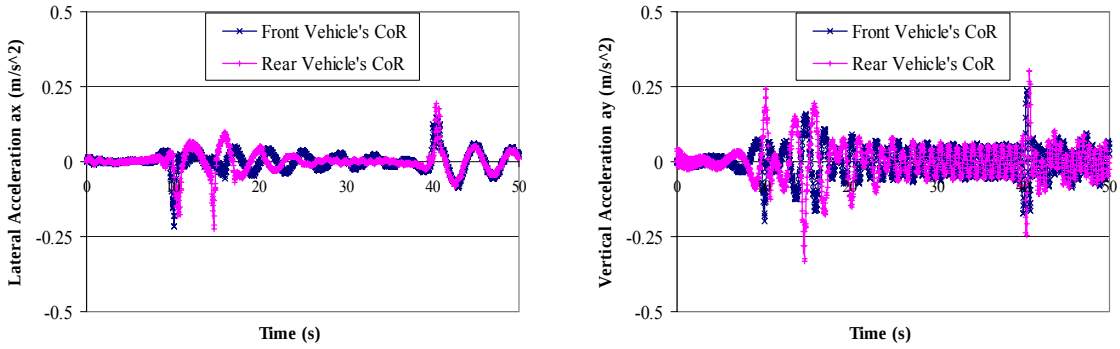

Fig. 10 Lateral and Vertical Accelerations of Front and Rear Vehicle's CoR

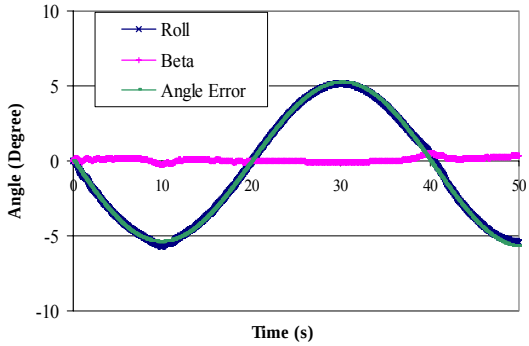

Fig. 11 Roll, Beta and Angle Error

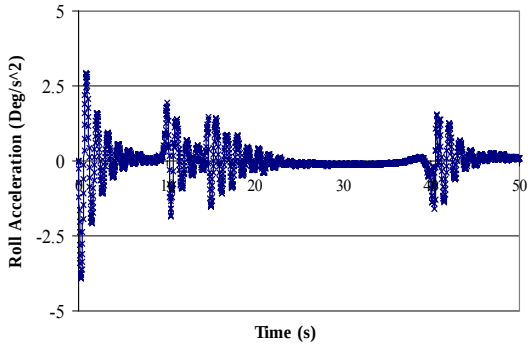

Fig. 12 Roll Accleration

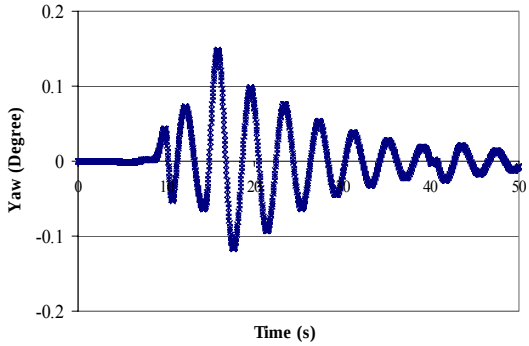

Fig. 13 Yaw Angle

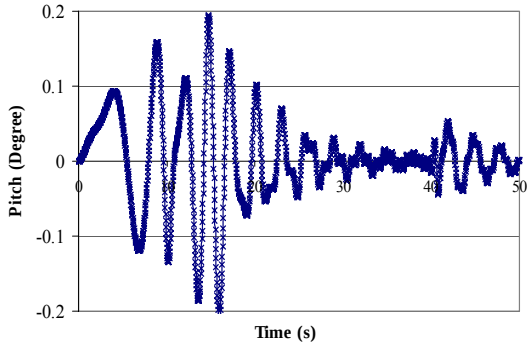

Fig. 14 Pitch Angle

As shown in Figure 12, roll accelertion will start to vibrate at the initial condition, at the two wind gusts and at the secondary suspension resonant zone. The maximum roll acceleration, however, is

only 4 deg/s^2, much less than the roll acceleration limitation of 15 deg/s^2 in curving performance [12]. Figure 13 and 14 show yaw and pitch angles. The maximum yaw angle is about 0.14 degree, and pitch angle 0.2 degree, which are very small comparing with the roll angle. We can therefore neglect both pitch angle and yaw angle in our control strategies, and can use a distributed control system to control both front and rear of the vehicle independently. Therefore, for acceleration feedback control, we need to measure accelerations of both front and rear vehicle's COR, and backfeed them, which reduces their accelerations significantly.

5 Conclusion

A 3D dynamic simulation model was developed to simulate and control the dynamic response of the magnetically levitated Magplane vehicle subject to periodic guideway disturbance, both vertical and lateral accelerations in curves, and strong side wind forces. A distributed control system was used to control the front and rear of the vehicle independently, and apply the acceleration feedback control and length compensation control in the active secondary suspension system of the lift pads to get good ride comfort quality. The roll angle closely follows the banking angle, and the propulsion windings can be kept in the center of guideway without need to tilt guideway at the banking angle.

6 References

1. Donald M. Rote and Yigang Cai. *Review of Dynamic Stability of repulsive-Force Maglev Suspension Systems,* IEEE Trans. On Magnetics, Vol. 38, No.2, March 2002, p1383-1390.
2. Magplane International, Inc. *System Concept Definition Report for the National Maglev Initiative,* Army Corps of Engineers Contract No. DTFR53-92-C-00006, September, 1992; 10 volumes, 1200 pages. Also see *Final Report on the National Maglev Initiative*, Report DOT/FRA/NMI-93/03, September, 1993.
3. Francis C. Moon. *Superconducting Levitation,* John Wiley & Sons, Inc, 1994.
4. Richard Thome, Alexi Radovinsky, and D. Bruce Montgomery. *EDS Levitation and Guidance Using Sheet Guideways*, 16th International Conference on Magnetically Levitated Systems and Linear Drives, Maglev'2000, Brazil, June, 2000, p236-241.
5. D. Bruce Montgomery, et al. *Electromagnetic Pipeline Demonstration Project*, 2nd International Symposium on Underground Freight Transportation, Delft, The Netherlands, September, 2000.
6. D. Bruce Montgomery. *Overview of the 2004 Magplane Design*, 18th International Conference on Magnetically Levitated Systems and Linear Drives, Maglev'2004, China, October, 2004.
7. S. Zhu, S. S. Chen, Y. Cai, and D. M. Rote. *Magnetic Damping for Maglev,* Active and Passive Control of Mechanical Vibration ASME, PVP-Vol. 289, 1994, p1-10.
8. Akio. Seki, Yutaka Osada, Jun-ichi Kitano, and Shigeki Miyamoto. *Dynamics of the Bogie of a Maglev System with Guideway Irregularities,* IEEE Trans. On Magnetics, Vol. 32, No.5, September 1996, p5043-5045.
9. S. Ohashi, H. Ohsaki, and E. Masada. *Magnetic Running Characteristics of the Magnetically Levitated Train in a Curved Track Section,* IEEE Trans. On Magnetics, Vol. 33, No.5, September 1997, p4212-4214.
10. Dunlap and Associates, Inc. *Development of Techniques and Data for Evaluating Ride Quality Volume II: Ride Quality Research,* 1978.
11. International Organization for Standardization. *Guide for the Evaluation of Human Exposure to Whole-Body Vibration,* 1974.
12. Department of Transportation (DOT). *Ride Comfort Guidelines,* DTFR53-92-C-00004, Appendix B, Section C, 1992.